International Journal of Rock Mechanics & Mining Sciences 54 (2012) 70–79

Contents lists available at SciVerse ScienceDirect

International Journal of Rock Mechanics & Mining Sciences

journal homepage: www.elsevier.com/locate/ijrmms

The impact of ellipsoidal particle shape on pebble breakage in gravel

Christoph Tuitz [a,*], Ulrike Exner [a,b], Marcel Frehner [a,1], Bernhard Grasemann [a]

[a] Department for Geodynamics and Sedimentology, University of Vienna, Austria
[b] Natural History Museum Vienna, Austria

ARTICLE INFO

Article history:
Received 1 March 2011
Received in revised form
8 May 2012
Accepted 14 May 2012
Available online 15 June 2012

Keywords:
Breakage load
Tensile stress
Weibull distribution
Finite element analysis
Point-load testing
Loading configuration

ABSTRACT

We have studied the influence of particle shape and consequently loading configuration on the breakage load of fluvial pebbles. Unfortunately, physical strength tests on pebbles, i.e., point-load tests, can only be conducted under one specific stable loading configuration. Therefore, the physical uniaxial strength tests performed in this study were extended by a two-dimensional finite-element stress analysis, which is capable of investigating those scenarios that are not possible in physical tests. Breakage load, equivalent to that measured in unidirectional physical tests, was determined from the results of the stress analysis by a maximum tensile stress-based failure criterion. Using this assumption, allows the determination of breakage load for a range of different kind of synthetic loading configurations and its comparison with the natural breakage load distribution of the physical strength tests. The results of numerical modelling indicated that the configuration that required the least breakage load corresponded with the minor principal axis of the ellipsoidal pebbles. In addition, most of the simulated gravel-hosted loading configurations exceeded the natural breakage load distribution of fluvial pebbles obtained from the physical strength tests.

1. Introduction

The study of sediment deformation is of great interest for disciplines concerned with near-surface geological processes such as soil mechanics, engineering geology and hydrogeology. Moreover, sediments affected by natural deformation processes, such as sand and gravel, are important commodities, extensively used in the construction industry and a common geological feature. Pebble breakage in gravel results in a change of pebble properties and microstructure and may therefore lead to several phenomena including (i) a decrease in permeability in both natural aquifers and industrial drainage-and filter systems, (ii) an increase in subsidence of buildings and constructions built on gravel foundations and (iii) a change of the mechanical bulk properties of gravel such as shear strength or stiffness [1].

Fluvial gravel deposits are mainly comprised of pebble sized aggregates (4–64 mm). The predominantly fluvial sediment transportation leads to a rounded ellipsoidal shape of the pebbles [2] and may also lead to preferred orientation of the longest axis of the pebbles. The specific shape of fluvial pebbles distinguishes them from many other more spherical and/or angular sedimentary particles in terms of their micro-mechanical response to bulk load, which is distributed and transferred over its particle contacts. The particle-shape may affect pebble rotation and translation in deformation bands [3], the packing density [4] or the contact force network and/or bulk strength [5,6]. The ellipsoidal pebble shape and its control on the stress distribution of potential loading configurations may also have a significant effect on the breakage tendency of pebbles and the investigation of this effect is the aim of this study.

Fractures are reported in imbricated pebbles of a natural fluvial gravel deposit [7]. Fig. 1 shows a section of a gravel layer from this outcrop that exhibits several pebbles with one or more fractures sub-parallel to the minor principal axes of the ellipsoidal pebbles. The fractures are Mode I, which indicates that the maximum tensile stress must have been perpendicular to the fracture plane and in this case also to the minor principal axis of the ellipsoidal pebbles. Hence, a preferred load transmission sub-parallel to the minor principal axes seems most likely.

This assumption is supported by two dimensional numerical studies of ellipse-shaped particle assemblies in biaxial compression [5]. Fig. 2b shows results of those studies indicating that force chains tend to be unidirectional and more localised in comparison to assemblies of spherical particles (Fig. 2a). Additionally, force chains in the assembly of ellipse-shaped particles are often oriented sub-parallel to the semi-minor axes of the ellipses. The numerical results show a clear link between the shape-controlled contact force network and the natural occurrence of fractures in imbricated fluvial pebbles. However, it is not clear if and to which extent the applied load that is necessary for breakage of an individual pebble varies with the position and orientation of the loading axis between two opposing contacts.

* Correspondence to: Christoph Tuitz, Department of Geodynamics and Sedimentology, University of Vienna, Austria, Althanstrasse 14, 1090 Vienna, Austria. Tel.: +43 1 4277 53478; fax: +43 1 4277 9534.
E-mail address: christoph.tuitz@univie.ac.at (C. Tuitz).
[1] Now at: Geological Institute, ETH Zurich, Switzerland.

1365-1609 © 2012 Elsevier Ltd. Open access under CC BY-NC-ND license.
http://dx.doi.org/10.1016/j.ijrmms.2012.05.018

The breakage load varies because the stress distribution inside irregular bodies is varying as a function of the loading geometry [8]. For the imbricated fluvial pebbles this could mean that they break more or less easily in the preferred loading direction relative to any other potential loading configuration. For example non-oriented pebble deposits may have no specific or a different preferred pebble loading orientation. This effect could influence the breakage rate of single pebbles in conjunction with the partitioning effect of the contact force network (Fig. 2) depending on the degree of pebble imbrication, but detailed investigations of this effect on ellipsoidal bodies, such as pebbles, have not yet been carried out.

The effect of shape on the internal stress distribution of bodies under non-uniform load is well known and reflected by the persistent standardisation of specimen shape for rock testing standards [9]. Remarkably, there are only two rock strength tests that allow testing of irregular shaped specimen, namely the point-load test (PLT) [10] and the Protodyakonov Impact Test [11], but both tests are greatly affected by scattering of the test results [12]. However, the point-load test is widely applied in science and industry, due to the small, simple and portable test equipment and rapid testing. The test yields the uncorrected point-load strength index (*Is*), which must be corrected to account for the specimen size to obtain the point-load strength index (e.g., Is_{50}) [13]. This index can then be used to estimate other rock strength parameters such as the unconfined compressive strength (*UCS*) or uniaxial tensile strength (*UTS*).

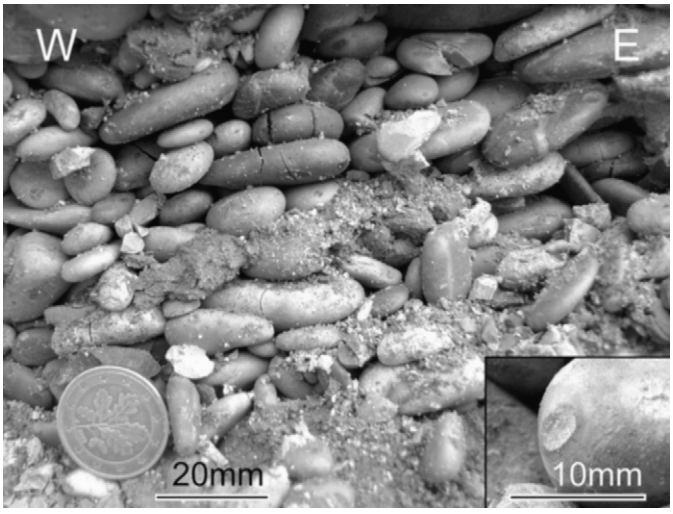

Fig. 1. Gravel layer at the outcrop from where samples were taken. Note a series of sub-parallel fractures in some pebbles, which are perpendicular to the longest principal axis of the pebbles. The inset shows a pebble with a solution pit at one of its former contacts.

In this study, fluvial pebble samples from a Miocene fluvial gravel deposit [14] were tested in the point-load test configuration for irregular specimens [12]. The resulting uncorrected point-load strength index, which is the force applied on the point load cones at catastrophic failure, of a large number of pebbles was statistically analysed. The non-standardized data was chosen for two principal reasons: First, the size of the pebbles was below the minimum size value recommended by the standard method for point-load testing [10,15]. On small samples, the contacts between the sample and the cones cannot be considered as theoretical points as in the case of standard point-load tests. Second, the point-load test configuration in this study is intended to mimic the contact geometry and loading configuration between pebbles in gravel, under central loading parallel to the minor principal pebble axis, and not to estimate rock strength properties such as *UCS* or *UTS*. The resulting distribution of breakage force values of the point-load tests, termed breakage load in this study, can be seen as a loading configuration specific test value that incorporates material and size variations of pebbles from a specific gravel sample.

Unfortunately, the ellipsoidal pebbles can only be tested in a centred position sub-parallel to the minor principal pebble axes, since this is the only stable test configuration. This problem was already recognised and described by Moss [16] for non-spherical quartz grains from fluvial sediments. In order to address this problem, finite element stress analyses were carried out in this study that allowed the investigation of different kinds of synthetic loading configurations, which are present in natural gravel deposits but difficult to achieve with standard point-load test devices. The numerically investigated loading configurations are: (i) translation of the loading axis parallel to the minor principal pebble axis, (ii) rotation of the loading axis around the centre and

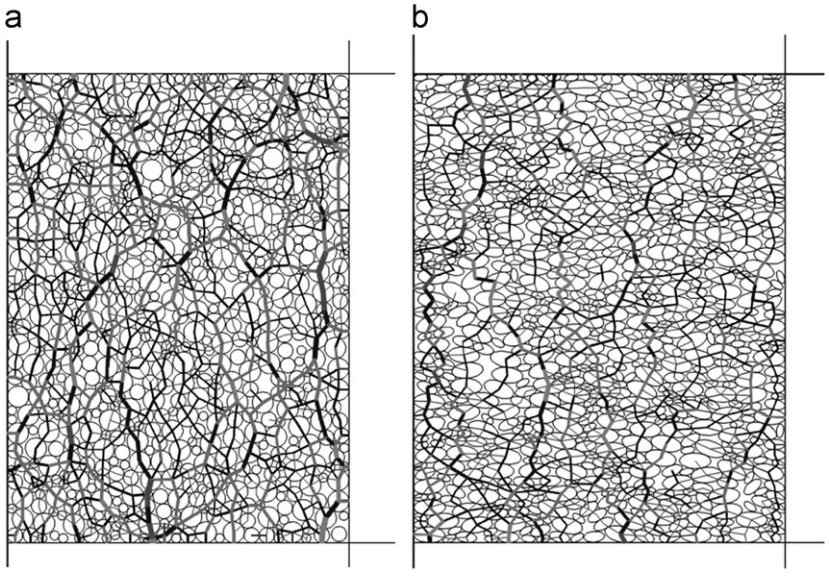

Fig. 2. Sphere- and ellipse-based discrete element method simulations of biaxial compression (after 10% shortening). The ellipsoidal particles in (b) have an aspect ratio of 2:1. Lines joining particle centres are normal forces; their thickness is proportional to force magnitude. (modified after [5]).

(iii) a combination of both. Additionally, the effect of pebble indentation (Fig. 1) and the effect of pebble ellipticity on the contact geometry were investigated. The stress analysis permits to study different loading configurations that are deviating from the stable point-load test configuration. However, the resulting stress variations cannot be directly related to breakage, unless some sort of failure law is assumed, i.e., failure occurs when the maximum tensile stress inside the pebble reaches the tensile strength of the pebble [17]. The variations of the resulting load necessary for breakage under different loading configurations can then be compared with each other and with the natural breakage load distribution of the pebbles. The results provide a better understanding of the impact of different shape-controlled loading configurations on single pebble breakage in fluvial gravel.

2. Sample material and point-load test statistics

2.1. Geological setting, sampling and material description

For this study a sampling site was found in a gravel pit south of St. Margarethen (Burgenland, Austria). The outcrop is located at the eastern margin of the Neogene Eisenstadt-Sopron Basin [18,19], a satellite basin of the Vienna Basin [20], and exposes deltaic gravel of Miocene age (11.9–11.6 Ma) [14]. The gravel is mainly composed of limestone pebbles (85%), but dolomite (5%), sandstone (5%) and quartz (5%) pebbles, also occur. At the sample site, some pebbles were fractured and a noticeable number of pebbles showed solution pitting at their contacts with neighbouring pebbles (Fig. 1).

The sampled sediment was portioned using a sediment splitter into a testable size of ~500 pebbles without altering the grain size distribution or the composition. The individual pebbles are well rounded, but exhibit a clear ellipsoidal shape (Fig. 1). The three principal axes of each pebble (i.e., D_S=shortest; D_I= intermediate, and D_L=longest axis) were measured with an accuracy of ± 0.1 mm. For the statistical analysis, the pebbles were grouped into classes according to their shortest axis (D_S ranges from 4 to 13 mm). Fig. 3 shows the distribution of pebble shape, for all sampled pebbles. The trend of the mean values of each size class reveals that the flatness ratio increases seriously, whereas the elongation ratio decreases only slightly with increasing grain size.

2.2. Strength testing

In the gravel deposit, the contact geometry of opposing pebbles is convex (sometimes with distinct solution pits; Fig. 1) and neighbouring pebbles exert a compressive contact load due to overburden. Therefore, the point-load configuration was an ideal laboratory configuration to reproduce the natural contact geometry and loading configuration and to determine the strength of pebbles, although only centred diametrical loading parallel to the shortest principal axis of the pebble is feasible.

In the applied strength tests, the pebbles were uniaxially compressed between two cone-shaped indenters [10] under dry conditions. The cone-shaped indenters were taken from a standard hand pump driven point-load test device and mounted on a computer-integrated uniaxial compression testing device (MCE QTS 100/100, Quicktest Prüfpartner GmbH, Langenfeld, Germany). This modification eliminates velocity variations by the hand drive and allows testing with a constant loading velocity. For each test a pebble was placed between two steel cones and shortened (loading velocity=0.5 mm/min) until pebble failure. All pebbles were tested parallel to the shortest axis, D_S, which is the only stable testing configuration. The breakage load is defined as the maximum load measured just before catastrophic failure.

It appears in Fig. 3 that no significant relationship between shape and breakage load exists. This is also illustrated by a plot of the elongation ratio (Fig. 4a) and flatness ratio (Fig. 4b) versus the binned breakage load. Both the mean values and the standard deviations of the shape ratios are nearly independent of breakage load, except for the last bin (5000–6000 N), which exhibit lower standard deviation. This observation, however, can be explained by a smaller sample size within this bin. Fig. 5 shows the relationship between the measured breakage load and the pebble size. A linear regression provides a good fit to the mean and the median values of the breakage load. The amount of data for pebble sizes >10 mm is decreasing and therefore the median values, which are more sensitive to this effect, deviate from the linear fit. The mean values are more robust and their deviation from the regression line is rather small. Furthermore, the

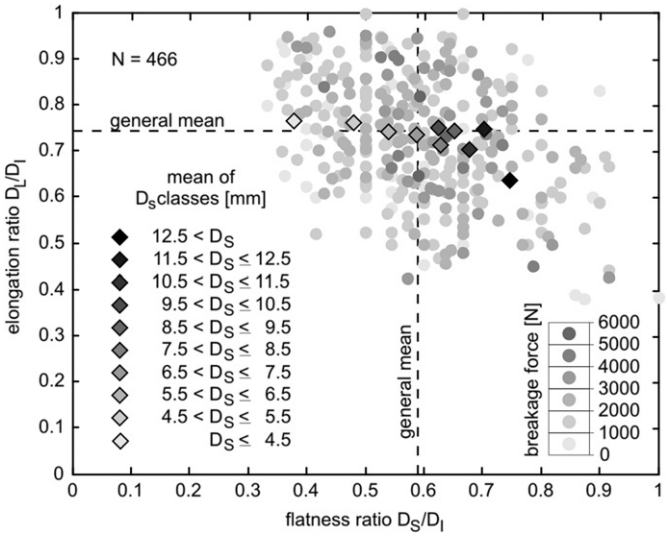

Fig. 3. Shape-plot of the sampled pebbles, illustrating the effect of pebble shape on breakage load (dots) in laboratory PLTs. Diamonds show the relation between shape and size of the tested pebbles. D_S is the smallest principal axis of the pebble.

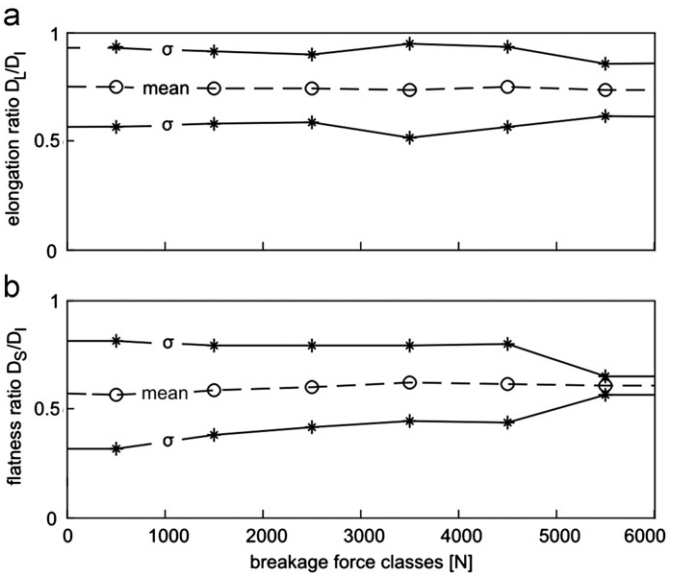

Fig. 4. Mean value and standard deviation of the elongation ratio (a) and the flatness ratio (b), for different classes of breakage load.

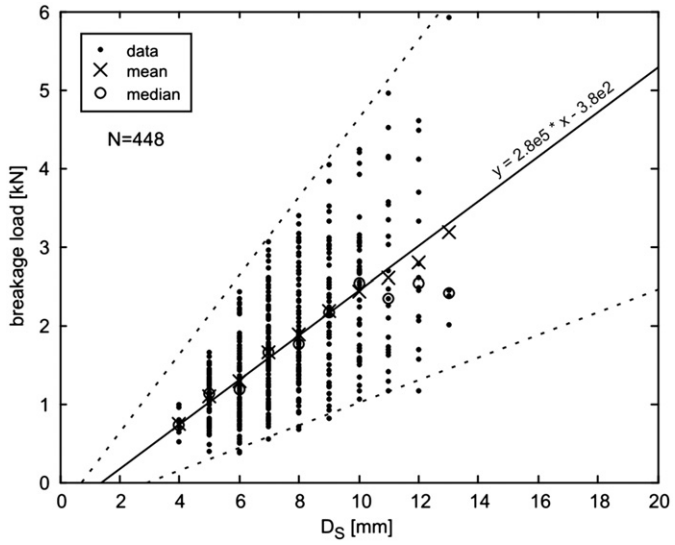

Fig. 5. Breakage load vs. pebble size from laboratory tests. The solid line is the linear regression of the class mean values with the given linear function. The dashed lines are the linear fits to the minimum and maximum values of each class.

minimum and maximum values of the breakage load data in each size class show a linear trend for pebble sizes >5 mm.

2.3. Mode of failure

In general, the pebbles fractured parallel to the applied load from one point-load cone to the other. The few tests in which the fracture plane did not pass both point-load cones were rejected. Samples of low breakage load often remained pinched between the cones or dropped next to the cones. Explosive fracturing was observed only for samples with high breakage load. Three pebble splitting types were observed: (i) 58% of the pebbles fractured along a median crack, with the majority approximately on the plane perpendicular to the longest axis, (ii) 22% of the pebbles fractured by the creation of a triple crack radiating from one of the point contacts and (iii) 20% of the pebbles fractured along numerous cracks producing more than three fragments. These three failure modes have also been observed in the studied gravel deposit.

2.4. Failure statistic

Since it is not clear from Fig. 5 how the breakage load values in each class are distributed, a statistical failure analysis for each class was performed separately. Pebble sizes <5 mm and >12 mm were not considered because few data exists. A two-parameter Weibull distribution [21] was fitted to the PLT results. The cumulative distribution function F of the two-parameter Weibull distribution has the form

$$F(F_B) = 1-\exp\left[-(F_B/\lambda)^{\alpha}\right], \quad (1)$$

where λ and α are the scale and the shape parameter of the distribution, respectively. The former corresponds to the value of the breakage load F_B at which the failure probability is 63.2%. So-called probability plots are used to determine the optimal parameters of the two-parameter Weibull distribution that fit the breakage load data of each size class best. A probability plot uses special axes that are scaled by a linearisation of the cumulative distribution function and the failure points are plotted by using median ranking. In this study Bernard's approximation [22], given by

$$MR = \frac{j-0.3}{N+0.4}, \quad (2)$$

was used to estimate the median ranks. The variable j is the failure order number and N is the total number of failures. Data are consistent with a two-parameter Weibull distribution if they plot on a straight line in the probability plot. The x-intercept and the slope of the fitted line indicate the scale and the shape parameter of the distribution, respectively.

Fig. 6a–h show the probability plots for the different size classes of the tested pebbles. For each class, a good linear fit to the data indicates that the distribution of the breakage load can be well described by a two-parameter Weibull distribution. This is supported by the high coefficients of determination for the different classes (Fig. 6i). The size classes from 6 mm to 11 mm (Fig. 6b–g) show a slight overestimation of the probability for low F_B-values. This was also observed by Lim [23], who attributed it to the existence of a minimum strength of the pebbles. It was proposed that pebbles that survive the grinding process at the quarry are the statistically stronger ones. In fact, this is also the case for fluvial pebbles, because disaggregation due to stream transportation leads to a statistical strength increase [16].

The two parameters of the Weibull distribution for the different size classes are summarised in Fig. 7. The scale parameter, λ, increases linearly with increasing pebble diameter. The shape parameter α with a mean value of 2.9 is approximately constant, except for the smallest two classes (4 mm and 5 mm). The higher α values in these two classes indicate a change from positively skewed symmetrical distributions, since the two-parameter Weibull distribution becomes symmetrical at a shape parameter of 4. However, the shape parameter of 5.4 for the 4 mm-class is probably an overestimate due to undersampling in this class.

3. Finite element stress analysis of different loading configurations

A finite element (FE) stress analysis was carried out to simulate different loading configurations, which allows full control over the boundary conditions and the geometrical setup and the calculation of the stress-tensor components at each desired point within a finite element of the numerical domain. As most pebble geometries are close to axisymmetric, a two-dimensional formulation was chosen.

3.1. Numerical method

The numerical code used in this study is a MATLAB implemented FE algorithm that was originally developed to simulate deformation of linear elastic media in two dimensions. In Frehner et al. [24] and Frehner and Schmalholz [25] the algorithm was applied to and successfully benchmarked for elastic wave-propagation in rocks. For the purposes of this study, the code was adapted and further developed. Calculations were performed on an unstructured numerical mesh consisting of 7-node isoparametric triangular elements with biquadratic continuous interpolation functions [26]. The unstructured triangular mesh was generated by the software Triangle [27], which produces high-quality Delaunay-type meshes. Numerical implementation of the FE method comprises the Galerkin weighted-residual method [26] and numerical integration on seven Gauss–Legendre quadrature points [28]. For solving the linear system of equations the standard direct solver provided by MATLAB was used. The output of the FE simulations is the displacement vector field, the

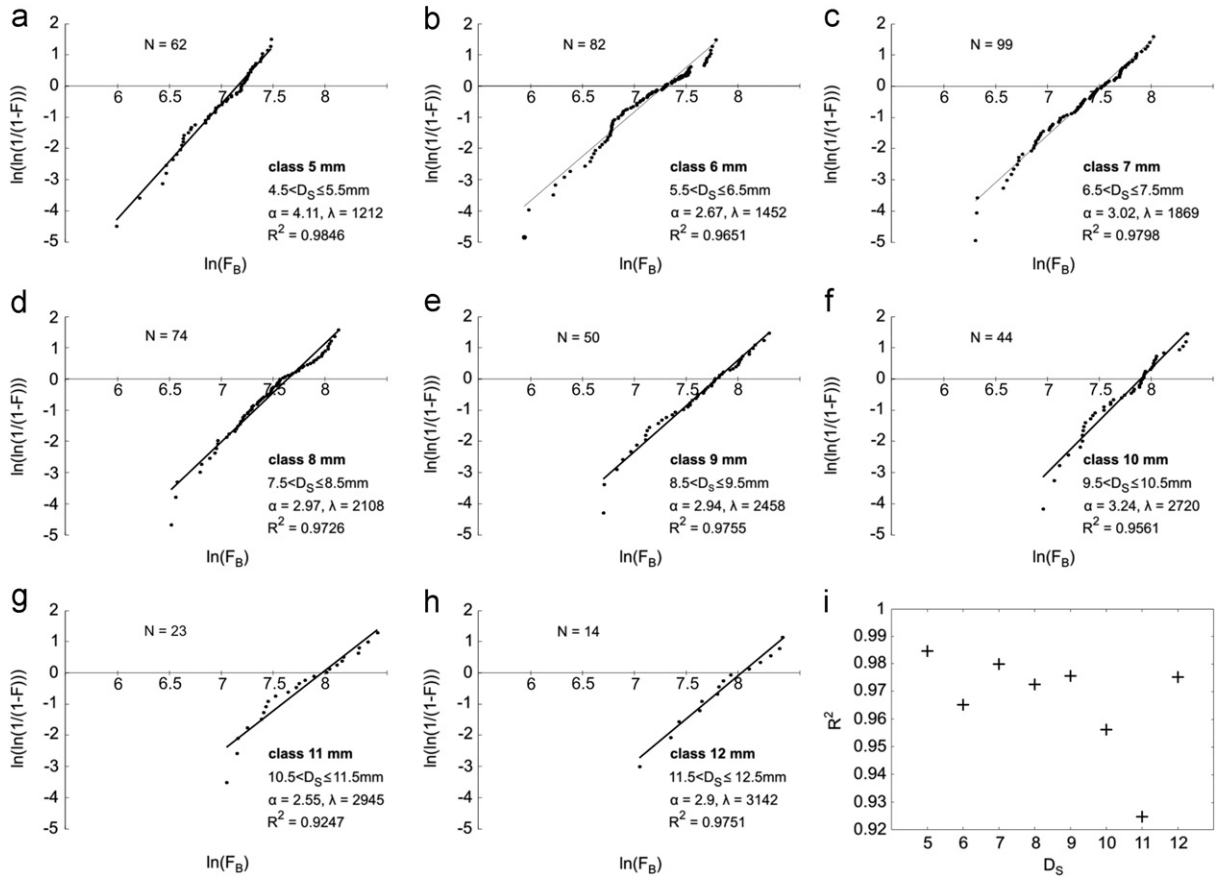

Fig. 6. Cumulative probability for eight grain size classes (a)–(h), calculated from median ranking for breakage load using the linearised two-parameter Weibull distribution [$\ln(\ln(1/(1-F)))$]. The solid lines represent the best linear fit for the data of each class. (i) Summary of the coefficients of determination of all classes.

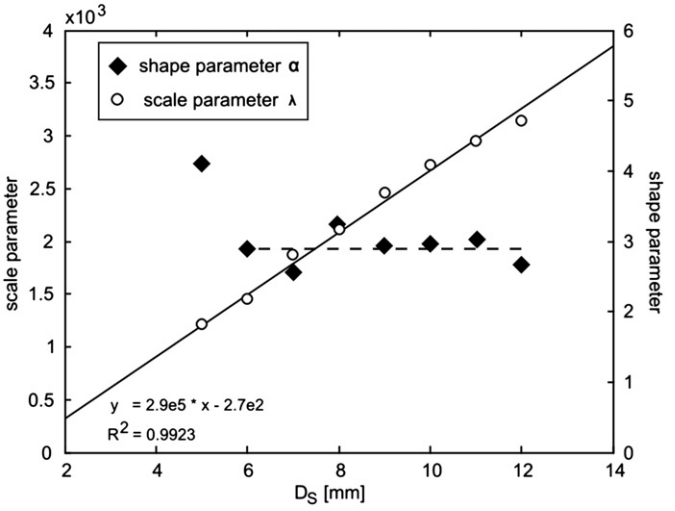

Fig. 7. Scale and shape parameters of the Weibull distribution vs. size class. The solid line is a linear regression to the class mean values of the scale parameter. The fitted dashed line indicates a fairly constant shape parameter for the classes above 5 mm.

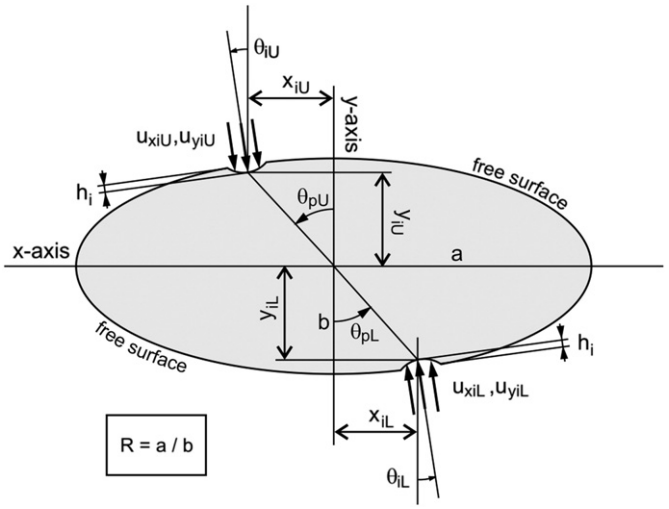

Fig. 8. Sketch (not to scale) of the numerical domain.

displacement gradient tensor field and the stress tensor field for the entire modelling domain.

The FE method is particularly well suited for analysing stresses in various diametrical loading configurations that are intended to extend and complement physical strength tests. On one hand, the unstructured mesh allows a very accurate approximation of the model geometry with strong spatial resolution variations over short distances in areas where higher resolution is required, e.g., towards the contact of the pebble with the loading cones. On the other hand, the FE formulation of the governing equations gives rise to the so-called natural boundary conditions. This special feature of the FE method allows a straightforward implementation of a shear stress-free surface, which is necessary when simulating strength tests of pebbles.

3.2. Model setups and boundary conditions

The elastic properties for all simulations were chosen according to the average properties of limestone (Young's modulus=45 GPa, Poisson ratio=0.25). The computational FE domain used in this study is shown in Fig. 8. It was defined as an ellipse with major and minor semi-axes a and b, respectively, whose dimension was except for the ellipticity analysis equivalent to the mean pebble dimension of the samples (a=8.6 mm, b=3.6 mm) for all simulations. The tips of the two point-load cones compressing the pebble in the physical strength tests were numerically represented by two small circular indenters with a radius of r_i=5 mm (same geometry as in standard point-load tests) [10]. The load in the physical strength tests is transmitted over a small area (relative to the particle size), rather than a mathematically defined point. Accordingly, the two contacts on the numerical pebble were defined as pits on the pebble surface geometry with an indentation depth of h_i (Fig. 8). Except for the indentation analysis, h_i was kept constant at 1% of the mean diameter of the pebble for all simulations. The locations of the lower and upper indenters are defined by the x- and y-distances from the centre to the contacts (x_{iL}, y_{iL} and x_{iU}, y_{iU}).

The boundary condition around the pebble is a traction-free boundary, except for the nodes at the contact locations of the two indenters. On these nodes a small displacement (i.e., $\ll h_i$) perpendicular to the tangent of the ellipse was prescribed. The indenter displacement u in the x- and the y-direction was defined as u_{xiL} and u_{yiL} for the lower and u_{xiU} and u_{yiU} for the upper indenter, respectively. The angle between this displacement vector and the y-axis is θ_i and the angle between the loading axis (axis connecting the two indenters) and the y-axis is θ_p (Fig. 8). The term standard loading configuration refers to the only stable loading configuration of the pebbles in the physical strength tests, i.e. the loading axis coinciding with the y-axis ($y_{iU}=b-h_i$, $y_{iL}=h_i-b$; $x_{iU}=x_{iL}=\theta_p=\theta_i=u_{xi}=0$).

3.3. Results of the stress analysis

Five different loading simulations that deviate from the standard loading configuration were analysed numerically. These are: (i) horizontal translation of the loading axis (Fig. 9a), (ii) rotation of the loading axis around the pebble centre (Fig. 9b, label A), (iii) combined translation and rotation of the loading axis (Fig. 9b, label B), (iv) changing initial indentation of the two indenters (Fig. 9c) and (v) changing ellipticity of the modelled pebble (Fig. 9d). For each configuration several stages within a realistic range of parameters were analysed. For all computations the magnitude of the displacement u was kept constant and the resulting maximum tensile stress in the model was calculated, which was in general located in the centre of the loading axis. In the graphs shown in Fig. 9 the variable parameter for each configuration is on the x-axis and the maximum tensile stress on the y-axis. Stresses are normalised by the standard loading configuration. In the following, the results for the different configurations are discussed separately.

In the case of a translation of the loading axis (i.e., $x_{iL}=x_{iU}=$ variable; $y_{iL}=f(x_{iL}, R)$, $y_{iU}=f(x_{iU}, R)$, $\theta_{pL}=f(x_{iL}, y_{iL})$, $\theta_{pU}=f(x_{iU}, y_{iU})$, $\theta_{iL}=f(\theta_{pL}, R)$, $\theta_{iU}=f(\theta_{pU}, R)$, $u_{xiL}=f(u, \theta_{iL})$, $u_{yiL}=f(u, \theta_{iL})$, $u_{xiU}=f(u, \theta_{iU})$, $u_{yiU}=f(u, \theta_{iU})$) the maximum tensile stress generally increased with horizontal translation (Fig. 9a). This increase was minor up to a translation of $x_{iU}=x_{iL}=0.5a$. After that the increase of the maximum tensile stress was more significant and reached a maximum value of 1.18 times the maximum tensile stress in the standard loading configuration at a translation of $0.83a$. The loading axis was only translated up to this point, since after this point the intenders cannot be considered as diametrically arranged.

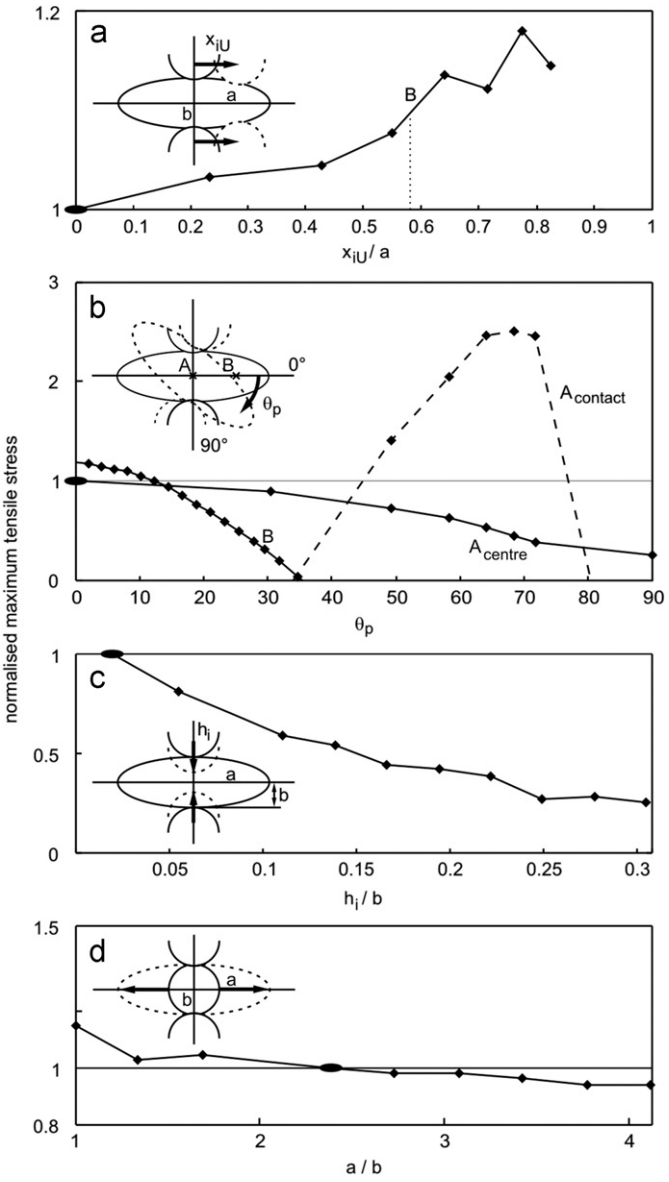

Fig. 9. Maximum tensile stress inside the numerical domain for different loading configurations and for constant displacement $u(x_i, y_i)$. All results are normalised to the standard loading configuration, which is indicated by a black ellipse.

In contrast to all other configurations, rotation of the loading axis (i.e., $\theta_{pL}=\theta_{pU}=$variable; $\theta_{iL}=f(\theta_{pL}, R)$, $\theta_{iU}=f(\theta_{pU}, R)$, $u_{xiL}=f(u, \theta_{iL})$, $u_{yiL}=f(u, \theta_{iL})$, $u_{xiU}=f(u, \theta_{iU})$, $u_{yiU}=f(u, \theta_{iU})$) indicated that for larger rotation angles the maximum tensile stress is not necessarily located in the middle of the loading axis, but adjacent to the indenter-contacts (Fig. 9b). Therefore, the tensile stress was measured at both locations, in the centre (solid line) and next to the indenter-contacts (dashed line). For small rotation angles the maximum tensile stress in the centre decreased slightly compared to the standard loading configuration. This decrease became more significant for rotation angles $>35°$. One of the principal stresses next to the indenter-contacts became tensile at a loading axis rotation angle of $\sim 35°$ and quickly increased with increasing rotation angle. At rotation angles $>42°$ it exceeded the tensile stress in the middle of the loading axis and reached a maximum value at a rotation angle of 68°. For rotation angles

$>80^\circ$ the maximum tensile stress adjacent to the indenter-contacts became less than the maximum tensile stress in the centre.

Combined translation and rotation of the loading axis (i.e., x_{iU}=variable, $x_{iL}=f(x_{iU})$, $\theta_{pL}=\theta_{pU}=f(x_{iL}, x_{iU})$, $y_{iL}=f(x_{iL}, R)$, $y_{iU}=f(x_{iU}, R)$, $\theta_{iL}=f(\theta_{pL}, R)$, $\theta_{iU}=f(\theta_{pU}, R)$, $u_{xiL}=f(u, \theta_{iL})$, $u_{yiL}=f(u, \theta_{iL})$, $u_{xiU}=f(u, \theta_{iU})$, $u_{yiU}=f(u, \theta_{iU})$) showed that the maximum tensile stress in the ellipse increased due to the translation of the loading axis (Fig. 9a), but decreased due to the rotation of the loading axis (Fig. 9b, label A). However, the increase of the maximum tensile stress as a function of the rotation around point *B* (Fig. 9b, label B) was much more significant than the increase due to the translation of the indenters to point *B*. Already after a rotation of 12° around point B, the decrease of the maximum tensile stress compensated for the increase due to the translation of the loading axis.

As the initial indentation of the two indenters increased (i.e., $y_{iL}=y_{iU}=$ variable; $x_{iL}=x_{iU}=\theta_{pL}=\theta_{pU}=\theta_{iL}=\theta_{iU}=u_{xiL}=u_{xiU}=0$; $u_{yiL}=u$, $u_{yiU}=-u$) the maximum tensile stress in the ellipse strongly decreased (Fig. 9c), but the rate of decrease became lower with increasing initial indentation. For the greatest tested initial indentation of 0.3*b* the maximum tensile stress in the ellipse only reached a value of 0.25 times the value for the standard loading configuration.

A change of ellipticity (i.e., a=variable; b=const., $y_{iU}=b-h_i$, $y_{iL}=h_i-b$, $x_{iL}=x_{iU}=\theta_{pL}=\theta_{pU}=\theta_{iL}=\theta_{iU}=u_{xiL}=u_{xiU}=0$), from a circle to an ellipse lead to a decrease of the maximum tensile stress with increasing ellipticity (Fig. 9d). For small aspect ratios the rate of decrease was higher and became almost negligible at an aspect ratio of ~3.5.

4. Loading configuration dependent variations of breakage load

In order to study the impact of different loading configurations deviating from central loading parallel to the minor principal axis on breakage load, the following assumptions were made: First, breakage is initiated when the maximum tensile stress inside the pebble reaches the tensile strength of the material, which is a criterion known as maximum tensile stress, or Rankine, criterion. Second, the carbonatic pebbles are isotropic in strength and behave like a linear elastic material. These assumptions allow determining the impact of any possible loading configuration on breakage load because the tensile strength of a specific pebble is independent of the loading configuration and the stress inside the pebble is linearly related to the contact load. In this case the breakage load that corresponds to a predefined constant stress (i.e., the tensile strength) of any loading configuration can be calculated from the linear relation between contact load and stress, as computed with the finite element method at different magnitudes of opposing displacements of the indenters $u_{(x_i,y_i)}$.

The statistical analysis of the strength test results on natural pebbles revealed a linear relation between the mean breakage load and pebble size D_S but similar distribution shapes in each size class. It is therefore possible to study both the deviation of the mean breakage load, and the deviation of the material dependent breakage load distribution for each size class. The results of the physical strength tests and the numerically determined breakage load are plotted in Fig. 10a–e, normalised by the breakage load for the standard loading configuration. In addition to the comparison of the numerical breakage load results among the different loading configurations, the plot enables the comparison of these results with the material dependent spread of the breakage load obtained by physical strength tests of fluvial pebbles.

In the case of translation of the loading axis (Fig. 9b) the mean breakage load decreases slightly to a breakage load of 0.85 times the breakage load in the standard loading configuration. The variation of the breakage load is much lower than the maxima and minima of the natural variation observed in physical strength tests and can therefore be regarded as insignificant. In the case of rotation (Fig. 9c), the change in breakage load is stronger but still insignificant compared to the natural variation for a rotation angle $<30^\circ$. For the case of combined translation and rotation (Fig. 9d) the breakage load increases significantly, and exceeds the natural variations of breakage load even at low rotation angles. An increase of initial indentation (Fig. 9e) has also a significant effect on the breakage load, showing an almost linear steep increase of the breakage load with increasing initial indentation. The change of breakage load with increasing ellipticity of the numerical domain (Fig. 9f) is relatively small. The breakage load only reaches a minimum normalised value of 0.8 and a maximum of 1.0, which is much smaller than the natural variation of breakage load.

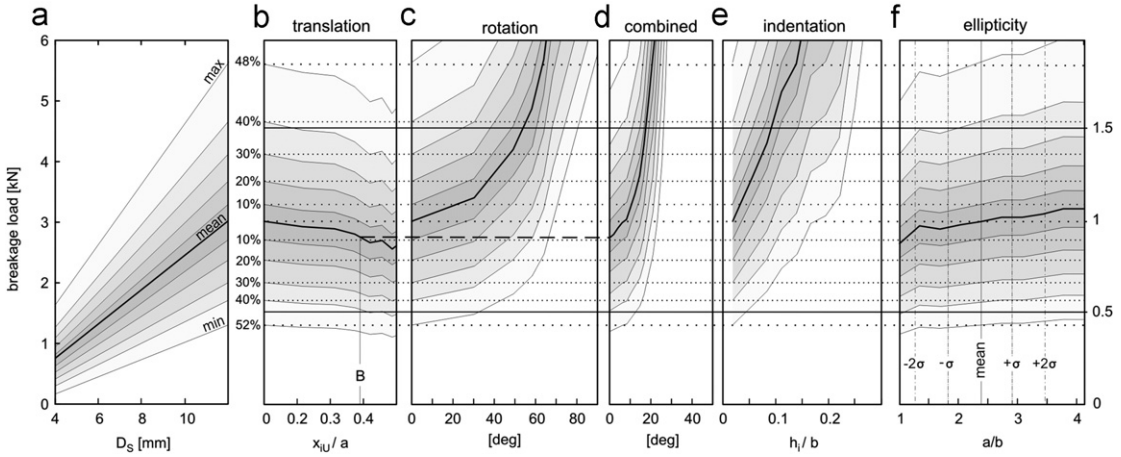

Fig. 10. Graphical evaluation of the impact of different loading configurations deviating from the standard loading configuration on the mean breakage load and on the natural breakage load distribution from physical PLTs. Subfigure (a) is a simplified version of Fig. 5. Subfigures (b)–(f) correspond to the configurations in Fig. 9(a)–(d), but now plotted as the breakage load necessary to reach a given critical tensile stress. The line in subfigure (b) denoted by *B* indicates the translational component of the combined case.

5. Discussion

5.1. Influence of geometric loading configuration on breakage load

The influence of the loading configuration on breakage presented in this study can be categorised into two main effects: (1) length change of the loading axis, and (2) change of the contact geometry between indenters and pebble (i.e., area and orientation).

In the physical strength tests on natural pebbles a linear relation between pebble size and the breakage load is observed (Fig. 5). In other words, the larger the pebble and therefore the longer the loading axis in the experiment is, the higher the pebble's resistance to breakage becomes. This linear relation supports the findings of Hiramatsu and Oka [29] that the stress fields along the loading axes are very similar for different specimen shapes.

This relationship can also be observed in the numerical FE simulations of different geometrical configurations. For example, if the loading axis is translated relative to the centre and subparallel to the minor principal pebble axis (Fig. 10b) then the loading axis becomes shorter and the breakage load decreases accordingly. However, this effect is minor, especially along the first half of the semi-axis a, because the length decrease of the loading axis is relatively small. This effect is supported by the fact that the fractures at the investigated outcrop (Fig. 1) are widely distributed around the centre and sometimes even develop a set of two or more parallel fractures. In contrast, in the case of rotation of the loading axis around the pebble centre (Fig. 10c), the loading axis lengthens rapidly with increasing rotation angle and hence, the breakage load increases rapidly. This effect is more pronounced for rotation around a point translated from the centre along the longest principal axes (Fig. 10d). However, because all these transformations (translation, rotation and the combination of the two) involve a slight change of the contact area and of the contact orientation, the resulting variations in the maximum tensile stress is a result of both the length change of the loading axis and the change of the contact geometry. Both pure translation of the loading axis and pure rotation around the centre of the ellipse are obviously theoretical configurations. In natural gravel it is much more likely that the loading configuration of a pebble leads to loading axes that are both translated from the centre and rotated relative to the principal axes of the pebble. Therefore, the results of the combined case (Fig. 10d) are considered more relevant for natural pebble breakage than the two theoretical end-members. They show a significant increase of the load necessary for breakage, even for small rotation angles of the loading axis.

The observed breakage load increase is much stronger for an increase of the initial indentation of the two numerical point load cones (Fig. 10c) as it is for pure translation and rotation. In this case slight shortening of the loading axis with increasing initial indentation is negligible, but the increase of the contact area between the indenters and the pebble gives rise to a major increase of the load necessary for breakage with increasing initial indentation. This contact area effect makes it difficult to relate the size of a pebble with its breakage load, because the contact geometry between the point load cones and the pebble plays such a significant role. Also, converting breakage load to tensile strength, which is often done via a simple particle size dependent function [9], may be strongly influenced by this effect. In addition to microstructural differences, this geometrical effect could also contribute to the relatively wide natural breakage load distribution, observed in physical strength tests (Fig. 5). The investigated indentation effect has a natural analogue in gravel deposits, since compressive contact loading may lead to solution pitting (Fig. 1). During this process, one of two neighbouring pebbles indents into the other by pressure and fluid induced mineral solution [30,31] and increases thereby the contact area between them. The results showed that at the same load the maximum tensile stress in pebbles with such contact geometries is lower than in pebbles with point-like contacts. In other words, pebbles that are preferentially loaded over contacts indicating significant solution pitting are harder to fracture than those ones with point-like contacts.

In the case of changing ellipticity (Fig. 10f) the length of the loading axis does not change, but the change of breakage load is due to the second effect, namely, an increase of the contact area between the indenters and the pebble with increasing ellipticity. The results in Fig. 9d show that the maximum tensile stress is decreasing with increasing ellipticity and therefore, a larger breakage load is necessary (Fig. 10f) to reach the critical tensile stress (i.e., tensile strength). In the case of ellipsoidal particles, this implies that the maximum tensile stress is larger perpendicular to the longest principal axis than perpendicular to the intermediate axis, which theoretically results in fractures that are preferably oriented perpendicular to the longest principal axis. This is in agreement with observation of fractured pebbles at the investigated outcrop where fractures are oriented preferably parallel to the surface defined by the shortest and intermediate axes within a deviation of $\pm 15^{\circ}$ (Fig. 1).

5.2. Failure criterion

To compare the breakage load of the different loading configurations with the standard loading configuration, a criterion was implemented that assumes failure to occur if the maximum tensile stress at the centre of the loading axis is reached. This assumption is justified by the fact that the fracture patterns of most of the broken pebbles at the outcrop do not exhibit near surface shear failure. Nevertheless, a study of near-surface shear stress development at the contacts for different loading configurations would be necessary for the general applications of the results to ellipsoidal bodies.

In this study failure is predicted if the maximum tensile stress in the numerical domain in any of the different loading configuration exceeds the maximum tensile stress measured in the standard loading configuration. Since this approach is based on the stress state at a point inside the domain, it does not take the size of the volume under tensile stress into account, which is known to have an effect on the strength of a specimen [32,33]. This phenomenon can be explained by the fact that larger volumes under tensile stress have a higher probability to enclose larger and therefore, failure-prone micro cracks (or in general defects). However, the carbonate pebbles in this study are composed of fine-grained calcite or dolomite (average, and maximum grain size of 0.1 mm and 0.5 mm, respectively) and exhibit a homogeneous microstructure with very few defects. The absence of large defects is not surprising, when fluvial transport is considered, which sorts weak pebbles (with defects) by fracturing and attrition, and leaves a residue of stronger components [16]. Therefore, the influence of volume size under tensile stress was neglected and crack initiation was assumed to be located close to the point of maximum tensile stress.

5.3. Multiple loading configurations

Natural pebbles are subjected to multiple contact loads (Fig. 1) and not only to two opposing contact loads, as in this study. Several studies [34–36] showed that in comparison to diametrically loaded spheres the stress distribution of circular discs and irregular shaped particles under multiple loads from

neighbouring particles changes significantly. Due to their confining effect the additional contact loads on spherical particles reduce the tensile stresses. However, the influence of multiple contact loads on the stress distribution and the breakage load of ellipsoidal shaped particles was not considered in this work. It is argued that the confining effect by multiple particle contacts for circular discs [34] has the same impact on the stress distribution of ellipsoidal pebbles in gravel, which have an aspect ratio $>2{:}1$. One potential argument is that the contact force networks in granular assemblies comprised of non-spherical particles show a stronger partitioning effect, into a strong and a weak force network, in comparison to spherical particle assemblies. Hence force chains are preferably oriented sub-parallel to the main loading direction [5,35]. Consequently, particles are loaded anisotropically and bear most of the load on a single loading axis or two sub-parallel loading axes with little load acting perpendicular to this main loading axis (Fig. 2b). In fact, the preferred orientation of fractures sub-parallel to the shortest principal axis and the occurrence of multiple sub-parallel fractures in single pebbles, especially for larger aspect ratios (Fig. 1), indicate that little confining load must have been present in the directions perpendicular to the main loading direction. However, even in the case that multiple contact loads would have a significantly strong confining effect on pebbles in gravel, the resultant relative change of breakage load for the different pebble loading configurations would be still valid, but their impact would be minor.

6. Conclusions

The aim of this study was to assess the breakage load of fluvial pebbles in gravel and to investigate its variability due to the different shape-controlled loading configurations. Physical strength tests on a pebble population from a suitable outcrop were conducted and statistically analysed. The physical test results were extended by means of numerical stress analysis, in which the influence of other loading configurations on breakage load that may occur in gravel, but are not practicable in physical strength tests, were investigated. The findings of the numerical analysis indicate that the load necessary for breakage has to increase if (i) the loading axes is rotated relative to the minor principal axes of the pebble, (ii) the loading axis is translated and rotated relative to minor principal axis of the pebble, (iii) the indentation of the pebbles increases (e.g., solution pitting) or (iv) the ellipticity of the pebble increases. Only pure translation of the contact loads parallel to the longest principal axis causes a minor decrease of breakage load. However, the impact differs depending on configuration type. The first two cases, translation parallel to the longest principal axis and rotation around the centre, show less effect on breakage load than the case in which these two components are combined. Since pure translation and pure rotation of the loading axis around the centre are rather theoretical configurations, the combined case is much more likely to occur in gravel and is therefore considered to be more relevant.

Furthermore, solution pitting, simulated by systematic variation of indentation, leads to a maximum tensile stress decrease and therefore to a higher breakage load compared to point-load like contacts. The effect of ellipticity indicates that the observed preferred fracture orientation perpendicular to the longest principal pebble axis is a result of the ellipsoidal shape. All studied configurations with a loading axis parallel to the smallest principal pebble axis lead to an increase of breakage load. In other words, the weakest configuration occurs when the loading axis coincides with the shortest principal axis and any deviation from this configuration except pure translation leads to an apparent strengthening of the pebble. These results are in accordance with fracture orientations measured at the outcrop. However, it is unlikely that loading axes generated in pebbles through neighbouring opposite pebbles in gravel coincide perfectly with the shortest principal pebble axis. In physical uniaxial strength tests the shortest principal pebble axis is also chosen to accomplish a stable loading configuration. Therefore, failure criteria based only on the results from simple uniaxial compression tests on particles with a pronounced ellipsoidal shape, as in the case of fluvial pebbles, are insufficient to determine particle breakage.

Acknowledgements

This work was funded by projects P20092-N10 and T325-N14 of the Austrian Science Fund (FWF). The Institute for Engineering Geology at the University of Vienna is thanked for using the rock mechanics laboratory. Stimulating discussions with A. Preh, M.P.J. Schöpfer, and B. Salcher improved this study considerably.

References

[1] Kokusho T, Hara T, Hiraoka R. Undrained shear strength of granular soils with different particle gradations. J Geotech Geoenviron 2004;130:621–9.
[2] Oakey RJ, Green M, Carling PA, Lee MWE, Sear DA, Warburton J. Grain-shape analysis—A new method for determining representative particle shapes for populations of natural grains. J Sediment Res 2005;75:1065–73.
[3] Exner U, Grasemann B. Deformation bands in gravels: displacement gradients and heterogeneous strain. J Geol Soc London 2010;167:905–13.
[4] Guises R, Xiang JS, Latham JP, Munjiza A. Granular packing: numerical simulation and the characterisation of the effect of particle shape. Granular Matter 2009;11:281–92.
[5] Ting JM, Meachum L, Rowell JD. Effect of particle-shape on the strength and deformation mechanisms of ellipse-shaped granular assemblages. Eng Comput 1995;12:99–108.
[6] Rothenburg L, Bathurst RJ. Influence of particle eccentricity on micromechanical behavior of granular materials. Mech Mater 1993;16:141–52.
[7] Decker K, Peresson H. Rollover and hanging-wall collapse during Sarmatian/Pannonian synsedimentary extension in the Eisenstadt Basin. Mitt Ges Geol Bergb Österr 1996;41:45–52.
[8] Tang CA, Liu HY, Zhu WC, Yang TH, Li WH, Song L, et al. Numerical approach to particle breakage under different loading conditions. Powder Technol 2004;143–4:130–43.
[9] Darvell BW. Uniaxial compression tests and the validity of indirect tensile-strength. J Mater Sci 1990;25:757–80.
[10] Bieniawski ZT. Point-load test in geotechnical practice. Eng Geol 1975;9:1–11.
[11] Protodyakonov MM. Mechanical properties and drillability of rocks. Proceedings of the 5th symposium rock mechanics. University of Minesota; 1963. p. 103–18.
[12] Broch E, Franklin JA. Point-load strength test. Int J Rock Mech Min Sci 1972;9:669–97.
[13] ISRM. Suggested method for determining pointload strength. Int J Rock Mech Min Sci 1985;22:51–60.
[14] Harzhauser M, Kowalke T. Sarmatian (Late Middle Miocene) gastropod assemblages of the Central Paratethys. Facies 2002;46:57–82.
[15] Franklin JA. Suggested method for determining point load strength. Int J Rock Mech Min Sci 1985;22:51–60.
[16] Moss AJ. Technique for assessment of particle breakage in natural and artificial environments. J Sediment Petrol 1972;42:725–8.
[17] Rankine WJM. On the stability of loose earth. Philos Trans R Soc London 1857;147:9–27.
[18] Schmid HP, Harzhauser M, Kroh A. Hypoxic events on a middle Miocene carbonate plattform of the central paratethys (Austria, Badenian, 14 Ma). Annalen des Naturhistorischen Museums in Wien 2001;102:1–50.
[19] Spahic D, Exner U, Behm M, Grasemann B, Haring A, Pretsch H. Listric versus planar normal fault geometry: an example from the Eisenstadt-Sopron Basin (E Austria). Int J Earth Sci 2011;100:1685–95.
[20] Royden LH. The Vienna basin: a thin skinned pull apart basin. In: Biddle KT, Christie-Blick N, editors. Strike slip deformation, basin formation and sediments. Tulsa: Society of Economic Paleontologists and Mineralogists; 1985. p. 310–38.
[21] Weibull W. A statistical distribution function of wide applicability. J Appl Mech 1951;18:293–7.
[22] Bernard A, Bos-Levenbach EC. The plotting of observations on probability paper. Stat Neerl 1953;7:163–73.
[23] Lim WL, McDowell GR, Collop AC. The application of Weibull statistics to the strength of railway ballast. Granular Matter 2004;6:229–37.

[24] Frehner M, Schmalholz SM, Saenger EH, Steeb H. Comparison of finite difference and finite element methods for simulating two-dimensional scattering of elastic waves. Phys Earth Planet Inter 2008;171:112–21.
[25] Frehner M, Schmalholz SM. Finite-element simulations of Stoneley guided-wave reflection and scattering at the tips of fluid-filled fractures. Geophysics 2009;75:T23–36.
[26] Zienkiewicz OC, Taylor RL. The finite element method—Volume 1: The basis. 5 ed. Oxford: Butterworth-Heinemann; 2000.
[27] Shewchuk JR. Delaunay refinement algorithms for triangular mesh generation. Comp Geom 2002;22:21–74.
[28] Hughes TJR. The finite element method: linear static and dynamic finite element analysis. Mineola, NY: Dover; 1987.
[29] Hiramatsu Y, Oka Y. Determination of the tensile strength of rock by a compression test of an irregular test piece. Int J Rock Mech Min Sci 1966;3:89–90.
[30] Tada R, Siever R. Pressure solution during diagenesis. Ann Rev Earth Planet Sci 1989;17:89–118.
[31] McEwen TJ. Brittle deformation in pitted pebble conglomerates. J Struct Geol 1981;3 25-&.
[32] Hardin BO. Crushing of soil particles. J Geotech Eng ASCE 1985;111:1177–92.
[33] Lade PV, Yamamuro JA, Bopp PA. Significance of particle crushing in granular materials—Closure. J Geotech Geoenviron 1996;123:889–90.
[34] Tsoungui O, Vallet D, Charmet JC. Numerical model of crushing of grains inside two-dimensional granular materials. Powder Technol 1999;105: 190–8.
[35] Liu HY, Kou SQ, Lindqvist PA. Numerical studies on the inter-particle breakage of a confined particle assembly in rock crushing. Mech Mater 2005;37: 935–54.
[36] Gallagher JJ, Friedman M, Handin J, Sowers GM. Experimental studies relating to microfracture in sandstone. Tectonophysics 1974;21:203–47.